Full paper/Mémoire

# Effect of pretreatment gases on the performance of WO$_3$/SiO$_2$ catalysts in the metathesis of 1-butene and ethene to propene

Huan Liu [a,b], Kai Tao [a], Hongbo Yu [a], Chen Zhou [a], Zhen Ma [c,*], Dongsen Mao [b,*], Shenghu Zhou [a,*]

[a] Ningbo Institute of Materials Technology and Engineering, Chinese Academy of Sciences, 1219, Zhongguan West Road, Ningbo, Zhejiang 315201, China
[b] Research Institute of Applied Catalysis, Shanghai Institute of Technology, 100, Haiquan Road, Shanghai 201418, China
[c] Department of Environmental Science and Engineering, Fudan University, Shanghai 200433, China

ABSTRACT

Different gases were employed to pretreat WO$_3$/SiO$_2$ for the metathesis of 1-butene and ethene to propene. Air-pretreated WO$_3$/SiO$_2$ was inactive, whereas N$_2$-, N$_2$/H$_2$-, and H$_2$-pretreated WO$_3$/SiO$_2$ exhibited high 1-butene conversion and propene selectivity. Tetragonal WO$_3$ and partially reduced WO$_{2.92}$ were found to be the active phases/species, whereas monoclinic WO$_3$ was inactive. N$_2$/H$_2$- and H$_2$-pretreated WO$_3$/SiO$_2$ contained both W$^{6+}$ and W$^{5+}$ species (i.e., nonstoichiometric WO$_{3-x}$). Air- and N$_2$-pretreated WO$_3$/SiO$_2$ only contained monoclinic W$^{6+}$ species (WO$_3$) before the reaction. However, the used N$_2$-pretreated WO$_3$/SiO$_2$ contained both W$^{6+}$ and W$^{5+}$ species, suggesting that the N$_2$ pretreatment can facilitate the formation of some W$^{5+}$ species during the reaction. This in situ partial reduction can activate the N$_2$-pretreated WO$_3$/SiO$_2$ for the metathesis.

© 2014 Académie des sciences. Published by Elsevier Masson SAS. All rights reserved.

## 1. Introduction

Olefin metathesis, first reported by Banks and Bailey in 1964 [1], is an important method for the production of fine chemicals and polymers [2–4]. Supported W [5–9], Mo [10–12], and Re [13,14] catalysts have been intensively studied for olefin metathesis. Among them, Re$_2$O$_7$/Al$_2$O$_3$ exhibits higher activity and selectivity at low reaction temperatures [15,16], but the high price of Re limits its wide applications. Although WO$_3$/SiO$_2$ is less active than Re$_2$O$_7$/Al$_2$O$_3$ and MoO$_3$/Al$_2$O$_3$, it is the most widely used in industry for the metathesis of butene and ethene due to its excellent stability and resistance to poisoning [17,18]. In a

typical process, 2-butene and ethene react to produce propene, and 1-butene in the butene mixture has to first isomerize to 2-butene in order to form propene [19]. Generally, a conversion of 65–70% and a propene selectivity of 90% were obtained on WO$_3$/SiO$_2$ at 250–300 °C, as reported by ABB Lummus [6]. MgO [19] was used together with WO$_3$/SiO$_2$ to isomerize 1-butene in the butene mixture to 2-butene in industrial processes.

The pretreatment conditions of supported WO$_3$ catalysts were found to influence the oxidation state of W, thus affecting its catalytic performance [20–24]. Choung and Weller pretreated WO$_3$/SiO$_2$ with N$_2$ or H$_2$ to form some WO$_{3-x}$ intermediates regarded as catalytically active species [25]. Westhoff and Moulijn found that slightly reduced WO$_3$/SiO$_2$ catalysts showed higher activity in metathesis than calcined samples, and a tungsten oxide composition between WO$_3$ and WO$_{2.95}$ (formed by H$_2$ reduction of WO$_3$/SiO$_2$ at 875 K) exhibited the highest

activity [26]. Basrur et al. inferred the formation of $WO_{2.9}$ through the appearance of a blue-violet color of the used catalyst, and $WO_{2.9}$ was regarded as the active species in metathesis [27]. Huang et al. reported that the activity of 10 W/Al$_2$O$_3$–x HY increased with the increase in the zeolite content (HY) [28]. When the zeolite content exceeded 70%, the activity decreased due to the deep reduction in $W^{6+}$ species. Zaki et al. reported that $WO_3$ could form three intermediate nonstoichiometric oxidation states ($WO_{2.96}$, $WO_{2.9}$, and $WO_{2.72}$) by $H_2$ reduction and the formation process could be adjusted by controlling the reduction conditions [29,30].

Although attempts have been made to explore the active species of $WO_3/SiO_2$ catalysts for the metathesis of 1-butene and ethene, there was no systematical investigation of the active species through comprehensive characterization and no systematical research about the effect of pretreatment gases on the catalytic performance. Herein, a systematical research about the change in the physicochemical properties of $WO_3/SiO_2$ pretreated by air, $N_2$, $N_2/H_2$, and $H_2$ was conducted by comprehensive characterization, and the catalytically active tungsten oxide phase/species were assigned. The correlation between the active tungsten oxide phase/species and the catalytic performance for the metathesis of 1-butene and ethene was concluded.

## 2. Experimental

### 2.1. Catalyst preparation

The $SiO_2$ support (surface area 399.1 m$^2$/g, size 3–5 mm) was obtained from Qingdao Haiyang Chemical Co. Ltd., and ammonium metatungstate (AR) was purchased from Sinopharm Chemical Reagent Co. Ltd. MgO tablets (surface area 78.13 m$^2$/g, size 4–5 mm) were prepared by direct compression of MgO powders (99.99%) purchased from Aldrich. $WO_3/SiO_2$ (6.0 wt% $WO_3$) was prepared by incipient-wetness impregnation of $SiO_2$ by an aqueous solution of ammonium metatungstate followed by drying at 120 °C for 12 h and calcination in the air at 460 °C for 4 h. The obtained catalyst, denoted as WS, will be further treated by different gases in a fixed-bed catalytic reactor.

### 2.2. Catalyst pretreatment process and catalytic testing

Nineteen grams of WS ($WO_3/SiO_2$ without any gas pretreatment) were blended with 76.0 g MgO tablets, and then loaded into a fixed-bed reactor (internal diameter 3.3 cm). The catalyst was first heated to 400 °C in $N_2$ with a flow rate of 1.0 L/min. At 400 °C, $N_2$, 1/9 $H_2/N_2$ (v/v), 1/1 $H_2/$ $N_2$ (v/v), or $H_2$ (flow rate 1.0 L/min) were fed into the reactor to treat the catalyst for 30 min. The reactor was further heated to 550 °C and maintained at 550 °C for 2 h under $N_2$ (flow rate 1.0 L/min). The reactor was then cooled down to 280 °C under $N_2$ (flow rate 1.0 L/min), followed by feeding 1-butene and ethene at 280 °C and 3.0 MPa, and at a weight hourly space velocity (WHSV, 1-butene + ethene) of 1.49 h$^{-1}$ with a 1.6/1.0 molar ratio of ethene/1-butene. The flow rate of ethene was monitored by a mass-flow controller, and 1-butene was pumped into the system and gasified in a preheater. The above catalysts pretreated by $N_2$, 1/9 $H_2/N_2$ (v/v), 1/1 $H_2/N_2$ (v/v), or $H_2$ were denoted as WS–$N_2$, WS–1/9H$_2$/N$_2$, WS–1/1H$_2$/N$_2$, or WS–$H_2$, respectively.

To obtain air-pretreated $WO_3/SiO_2$ (WS–air), WS blended with MgO was first heated to 400 °C in the air (flow rate 1.0 L/min). At 400 °C, air (flow rate 1.0 L/min) was fed into the reactor to treat the catalyst for 30 min. The reactor was further heated to 550 °C and maintained at 550 °C for 2 h under air (flow rate 1.0 L/min) to get rid of residual water. The reactor was then cooled down to 280 °C under air (flow rate 1.0 L/min), which was followed by feeding the reactants. The reaction conditions for WS–air were the same as those described above.

The reaction products were analyzed online using a gas chromatograph equipped with a flame ionization detector (FID), and 1-butene conversion and propene selectivity were calculated according to the literature [28,31].

### 2.3. Catalyst characterization

Inductively coupled plasma (ICP) analysis was performed on a PerkinElmer OPTIMA 2100 DV optical emission spectroscopy spectrometer to identify the real tungsten oxide contents in the $WO_3/SiO_2$ catalysts. Brunauer–Emmett–Teller (BET) surface areas, pore volumes, and pore sizes were obtained using a Micromeritics ASAP 2020 M adsorption apparatus. Prior to measurement, the sample was degassed under vacuum at 200 °C for 3 h. X-ray diffraction (XRD) patterns were recorded with a D8 Advance X-Ray Diffractometer using Cu Kα radiation in the 2θ range from 10° to 70°. Raman spectra were obtained using a Renishaw Raman Spectrometer equipped with a microscope (laser wavelength: 532 nm). UV–vis spectra were recorded using a PE Lambda950 with $BaSO_4$ as a reference.

The images of transmission electron microscopy (TEM) and high-resolution transmission electron microscopy (HRTEM) were recorded on a Tecnai F20 Transmission Electron Microscope. The samples were prepared as follows: the catalysts were dispersed in ethanol by sonication, and a few drops of the dispersion were dropped onto a carbon-coated copper grid, which was followed by solvent evaporation in the air at room temperature.

X-ray photoelectron spectroscopy (XPS) data were recorded by a Kratos AXIS ULTRA DLD X-ray photoelectron spectrometer using Al Kα as the exciting source. Data processing was performed using CasaXPS software. The spectra were fit after linear background subtraction.

$H_2$ temperature-programmed reduction ($H_2$-TPR) was carried out in a quartz microreactor. The as-prepared samples (50 mg) were pretreated at 300 °C in Ar for 1 h prior to $H_2$-TPR measurement, which was followed by a temperature-programmed reduction by 1/10 $H_2$/Ar flow (v/v, 50 mL/min) from room temperature to 800 °C with a ramping rate of 5 °C/min. Hydrogen consumption was monitored by a thermal conductivity detector (TCD).

The infrared (IR) spectra of the samples were obtained in a transmission mode in a Bruker Tensor 27 spectrophotometer. A Pyris Diamond thermogravimetric analyzer

**Table 1**
Specific surface areas, pore volumes, and mean pore sizes of $WO_3/SiO_2$ catalysts pretreated by different gases.

| Catalysts | BET surface area (m²/g) | Pore volume (cm³/g) | Average pore size (nm) |
|---|---|---|---|
| WS–air | 332 | 0.83 | 7.5 |
| WS–N₂ | 345 | 0.83 | 7.2 |
| WS–1/9H₂/N₂ | 344 | 0.84 | 7.3 |
| WS–1/1H₂/N₂ | 339 | 0.89 | 8.3 |
| WS–H₂ | 349 | 0.88 | 7.8 |

(TGA) was used to analyze the organic residues in the used catalysts. The experimental run was carried out from 50 to 800 °C with a heating rate of 10 °C/min in flowing air (flow rate 50 mL/min).

## 3. Results and discussion

The BET surface areas, pore volumes, and mean pore sizes of $WO_3/SiO_2$ catalysts with an actual $WO_3$ content of 6.0 wt% determined by ICP are summarized in Table 1. All catalysts after different gas pretreatments showed insignificant changes of BET surface areas, and a slight change in pore volume and pore size was found in $1/1H_2/N_2$ and $H_2$-pretreated catalysts.

XRD patterns of $WO_3/SiO_2$ catalysts are shown in Fig. 1. As shown in Fig. 1b and 1c, WS-air and WS-N₂ exhibited similar XRD patterns assigned to monoclinic $WO_3$. In contrast, WS–1/9H₂/N₂ (Fig. 1d) and WS–1/1H₂/N₂ (Fig. 1e) exhibited XRD patterns assigned to tetragonal $WO_3$, suggesting that the thermal treatment of WS in the presence of $H_2/N_2$ mixtures induced the phase change of $WO_3$. When pure $H_2$ was used to pretreat WS, nonstoichiometric $WO_{2.92}$ phase appeared (Fig. 1f), indicating the partial reduction of $WO_3$ [29].

XPS data of $WO_3/SiO_2$ after different gas pretreatments are shown in Fig. 2. The XPS curve fitting procedure is that of Doniach and Sunjic [32]. The binding energies of
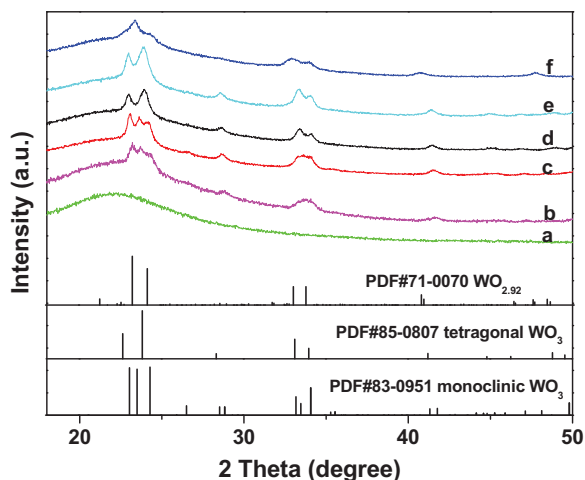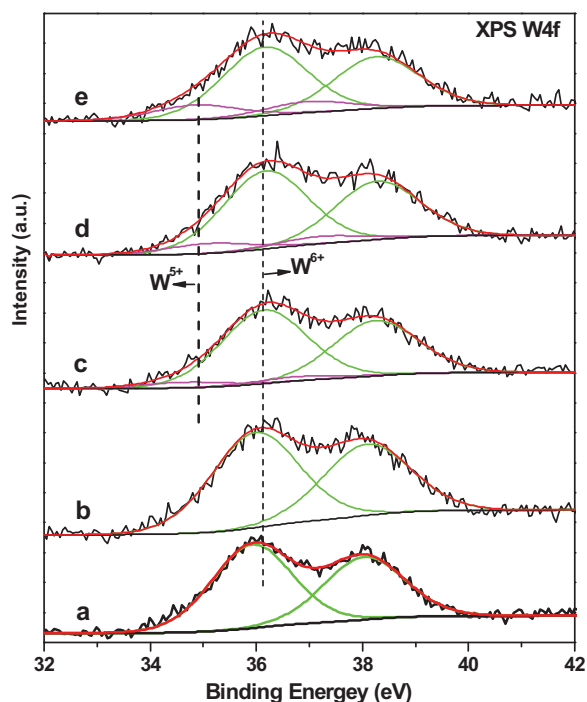


**Fig. 2.** (Color online.) XPS spectra of 6.0 wt% $WO_3/SiO_2$ catalysts pretreated with different gases: (a) WS–air; (b) WS–N₂; (c) WS–1/9H₂/N₂; (d) WS–1/1H₂/N₂; (e) WS–H₂.

35.9 and 38.0 eV in Fig. 2a for WS–air were assigned to $4f_{7/2}$ and $4f_{5/2}$ of $W^{6+}$ ($WO_3$), respectively [33–35]. As shown in Fig. 2b, WS–N₂ exhibited the similar XPS data as WS–air; only $W^{6+}$ was observed. For WS–1/9H₂/N₂, WS–1/1H₂/N₂, and WS–H₂, in addition to the binding energies of $W^{6+}$, the binding energies of 34.6~35.1 eV and 36.7~37.2 eV can be assigned to $4f_{7/2}$ and $4f_{5/2}$ of $W^{5+}$ [36–39], respectively, confirming the partial reduction of a small portion of $WO_3$ by $H_2$ or $H_2/N_2$ pretreatment. The intensities of XPS peaks of $W^{5+}$ increased with the increase in the $H_2$ content in the gases.

Table 2 summarizes the molar percentages of $W^{6+}$ and $W^{5+}$ obtained by XPS for different gas-pretreated $WO_3/SiO_2$. $W^{5+}$ did not exist in WS–air and WS–N₂, while $W^{5+}$ was observed in the catalysts pretreated by $H_2$ or $H_2/N_2$. When the $H_2/N_2$ ratio was increased from 1/9 to 1/1, the molar percentage of $W^{5+}$ increased from 7.1% to 11.3%. For WS–H₂, the molar percentage of $W^{5+}$ approached



**Fig. 1.** (Color online.) XRD patterns of 6.0 wt% $WO_3/SiO_2$ catalysts pretreated with different gases: (a) commercial $SiO_2$, (b) WS–air; (c) WS–N₂; (d) WS–1/9H₂/N₂; (e) WS–1/1H₂/N₂; (f) WS–H₂.

**Table 2**
Binding energies and molar percentages of $W^{5+}$ and $W^{6+}$ species in $WO_3/SiO_2$ catalysts pretreated by different gases.

| Catalysts | Binding energies for $W_{4f}$ (eV) | | | | $W^{5+}$ (%) | $W^{6+}$ (%) |
|---|---|---|---|---|---|---|
| | $W^{6+}$ $4f_{5/2}$ | $W^{6+}$ $4f_{7/2}$ | $W^{5+}$ $4f_{5/2}$ | $W^{5+}$ $4f_{7/2}$ | | |
| WS–Air | 38.0 | 35.9 | N/A | N/A | 0.0 | 100.0 |
| WS–N₂ | 38.1 | 36.0 | N/A | N/A | 0.0 | 100.0 |
| WS–1/9H₂/N₂ | 38.2 | 36.1 | 36.7 | 34.6 | 7.1 | 92.9 |
| WS–1/1H₂/N₂ | 38.2 | 36.1 | 37.2 | 35.1 | 11.3 | 88.7 |
| WS–H₂ | 38.2 | 36.1 | 36.9 | 34.8 | 17.7 | 82.3 |

17.7%. The relationship between the content of $W^{5+}$ and the pretreatment gas was first reported here.

The $WO_3/SiO_2$ catalysts pretreated by different gases were studied by Raman spectroscopy. Raman peaks at 806, 710, and 268 $cm^{-1}$ in Fig. 3, were assigned to the symmetric stretching mode of W–O, the bending mode of W–O, and the deformation mode of W–O–W in crystalline $WO_3$, respectively [40,41]. Moreover, a band around 979 $cm^{-1}$ was assigned to the O=W=O bond of the isolated surface tetrahedral tungsten oxide [42–44]. In this work, WS–air in Fig. 3a and WS–$N_2$ in Fig. 3b exhibited characteristic Raman bands at 806, 710, and 268 $cm^{-1}$, corresponding to crystalline $WO_3$. For WS–1/9$H_2$/$N_2$ (Fig. 3c) and WS–1/1$H_2$/$N_2$ (Fig. 3d), the Raman peaks at 806 $cm^{-1}$ became broader, and the peaks at 710 and 268 $cm^{-1}$ disappeared, suggesting a gradual degradation of $WO_3$ crystallinity [45]. For WS–$H_2$ in Fig. 3e, all the Raman peaks of crystalline $WO_3$ almost disappeared, which is consistent with the reported Raman spectra of $WO_{2.9}$ [46]. The band at 979 $cm^{-1}$ indicated the presence of isolated surface tetrahedral tungsten oxide in WS–air, WS–$N_2$, WS–1/9$H_2$/$N_2$, and WS–1/1$H_2$/$N_2$.

UV–vis DRS spectra of $WO_3/SiO_2$ pretreated by different gases are shown in Fig. 4. All catalysts showed two absorption bands at 215 and 250 nm, assigned to isolated $[WO_4]^{2-}$ tetrahedral species and octahedral polytungstate species, respectively [47–49]. Huang et al. and Zhao et al. ascribed the absorption between 400 and 800 nm to reduced W species such as $W^{4+}$ and $W^{5+}$ [28,31]. In our present work, the absence of absorption between 450 and 800 nm in Fig. 4a and 4b indicated that W species in WS–air and WS–$N_2$ were in the $W^{6+}$ state, which is consistent with the XRD and XPS results. For the $H_2$/$N_2$ or $H_2$-pretreated catalysts, the intensity of the band between 450 and 800 nm increased with the increase in $H_2$ content, suggesting the increase of the content of partially reduced W species, which is consistent with the XPS results. The formation of partially reduced W species by $H_2$ reduction of $WO_3/SiO_2$ allows the
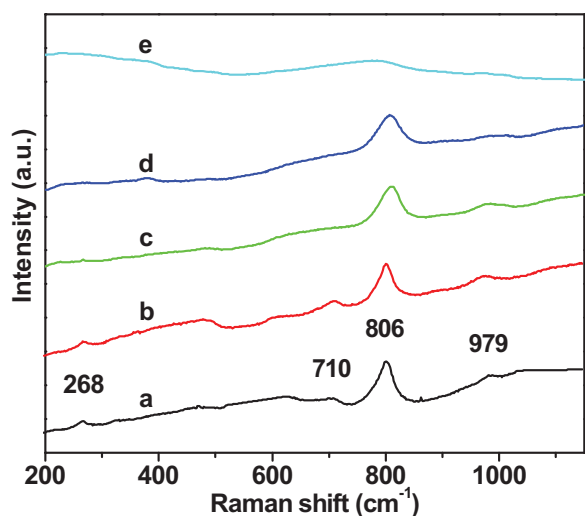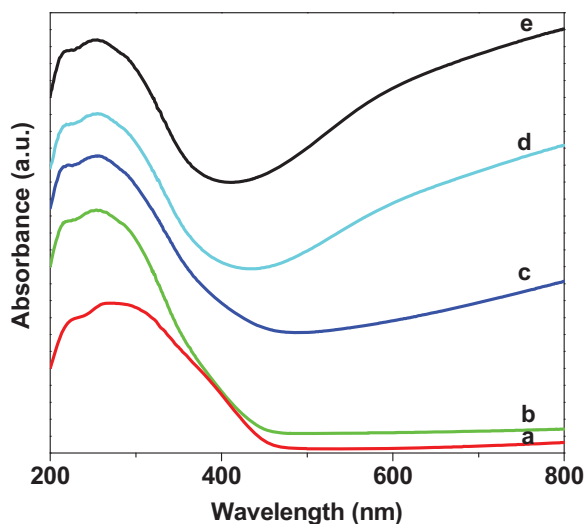
Fig. 4. (Color online.) UV–vis spectra of 6.0 wt% $WO_3/SiO_2$ catalysts pretreated with different gases: (a) WS–air; (b) WS–$N_2$; (c) WS–1/9$H_2$/$N_2$; (d) WS–1/1$H_2$/$N_2$; (e) WS–$H_2$.

intervalence charge transfer from $W^{5+}$ to $W^{6+}$ in the substoichiometric $WO_{3-x}$ [50], which explains the observation that the color of the catalyst gradually changed from yellow ($WO_3$) to deep blue ($WO_{2.92}$).

$H_2$-TPR was used to monitor the reduction process of WS–air, WS–$N_2$, and WS–1/1$H_2$/$N_2$. As shown in Fig. 5a, the main $H_2$ consumption peak for WS–air was observed at 602–711 °C, with a very slight hump of $H_2$ consumption centered at 450 °C, while the first obvious $H_2$ consumption peak for WS–$N_2$ in Fig. 5b was at 417–520 °C, suggesting that WS–$N_2$ was more easily partially reduced by $H_2$ than WS–air. For WS–1/1$H_2$/$N_2$ in Fig. 5c, the first $H_2$ consumption peak was further shifted to lower temperatures starting at ca. 400 °C, indicating the easiest reducibility of WS–1/1$H_2$/$N_2$.

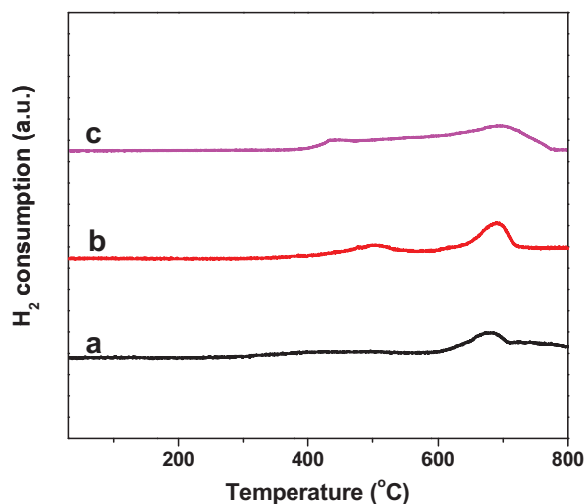Fig. 3. (Color online.) Raman spectra of 6.0 wt% $WO_3/SiO_2$ pretreated with different gases: (a) WS–air; (b) WS–$N_2$; (c) WS–1/9$H_2$/$N_2$; (d) WS–1/1$H_2$/$N_2$; (e) WS–$H_2$.

Fig. 5. (Color online.) $H_2$–TPR profiles of the pretreated 6.0 wt% $WO_3/SiO_2$ catalysts: (a) WS–air; (b) WS–$N_2$; (c) WS–1/1 $H_2$/$N_2$.

In the literature, the deep reduction of $WO_3/SiO_2$ catalysts was reported to be unfavorable to butene and ethene metathesis [28,51]. From the $H_2$-TPR data (Fig. 5), we can see that the deep reduction of catalysts occurred above 600 °C. That is the reason why we pretreated the catalysts (in air, $N_2$, $1/1H_2/N_2$, $1/9H_2/N_2$, or $H_2$) consistently at 400 °C. XPS data in Table 2 also confirmed that $W^{6+}$ can be partially reduced to $W^{5+}$ at 400 °C by $H_2/N_2$ or $H_2$, and the ratio of $W^{5+}/W^{6+}$ can be adjusted by the ratio of $H_2/N_2$, thus providing opportunities for studying the effect of these parameters on catalytic performance.

TEM images of $WS–N_2$ and $WS–1/1H_2/N_2$ are shown in Fig. 6a and 6b, respectively. $WO_3$ particles were clearly observed on $SiO_2$. The HRTEM images of $WS–N_2$ and $WS–1/1H_2/N_2$ are shown in Fig. 6e and 6f, respectively. The lattice spacing (0.363 nm) of $WS–N_2$ in Fig. 6e is consistent with that of (200) planes of monoclinic $WO_3$ detected by XRD in Fig. 1c. Moreover, the lattice spacing with 0.392 nm of $WS–1/1H_2/N_2$ in Fig. 6f is consistent with that of (001) planes of tetragonal $WO_3$ detected by XRD in Fig. 1e.

The catalytic performance of $WO_3/SiO_2$ catalysts with different gas pretreatments was tested for metathesis of 1-butene and ethene in a fixed-bed reactor. The catalysts first converted 1-butene to 2-butene, and further catalyzed the metathesis of 2-butene and ethene to propene. In industrial processes, the reactant butene contains 1-butene and 2-butene, and MgO is used to convert the 1-butene fraction to 2-butene in order to obtain high product yield. In this study, $WO_3/SiO_2$ catalysts blended with MgO tablets were used for reaction testing. Below, the real catalyst systems were the $WO_3/SiO_2$ catalysts with MgO, unless otherwise specified.

To begin with, MgO was tested in the reaction to investigate the role of MgO. As shown in Fig. 7a, 34.2% conversion of 1-butene was achieved on MgO, and no propene was detected, suggesting that the only role of MgO was to convert 1-butene to 2-butene.

$WS–1/1H_2/N_2$ (without MgO) showed an average conversion of about 60% and an average propene selectivity of 74% during 5 h on stream (Fig. 7b). $WS–1/1H_2/N_2$ blended with MgO exhibited an average conversion of ca. 80% and an average propene selectivity of 89% (Fig. 7c). The enhancement in 1-butene conversion for the MgO-blended $WO_3/SiO_2$ is due to the extra 1-butene conversion provided by MgO. The increase in propene selectivity with the addition of MgO is due to the fact that MgO decreases the concentration of 1-butene, thus minimizing the formation of the high-molecular-weight compound via 1-butene oligomerization [52].

The catalytic performances of $WO_3/SiO_2$ with different gas pretreatments are summarized in Table 3, in which the product was sampled for online analysis at 2 h on stream. $WS–air$ showed 33.5% of 1-butene conversion and 0.0% of propene selectivity, nearly the same as that of MgO, suggesting that $WS–air$ was inactive. In contrast, $WS–N_2$ showed a conversion of 75.0% and a propene selectivity of 84.1%. All the $H_2$- and $H_2/N_2$-pretreated catalysts exhibited enhanced 1-butene conversion and propene selectivity. Among them, $WS–1/1H_2/N_2$ exhibited the highest 1-butene conversion and propene selectivity.

The propene yield (conversion × selectivity) of $WO_3/SiO_2$ catalysts decreased in the following order: $WS–1/1H_2/N_2$ (79.7%) > $WS–H_2$ (75.5%) > $WS–1/9H_2/N_2$ (66.8%) > $WS–N_2$ (63.1%) > $WS–air$ (0.0%). Although $WS–N_2$ and $WS–air$ exhibited similar XRD, XPS, Raman, and UV–vis data, $WS–N_2$ exhibited excellent 1-butene conversion and propene selectivity, whereas $WS–air$ was inactive, indicating the formation of some active $WO_3$ phase and W species during metathesis on $WS–N_2$.

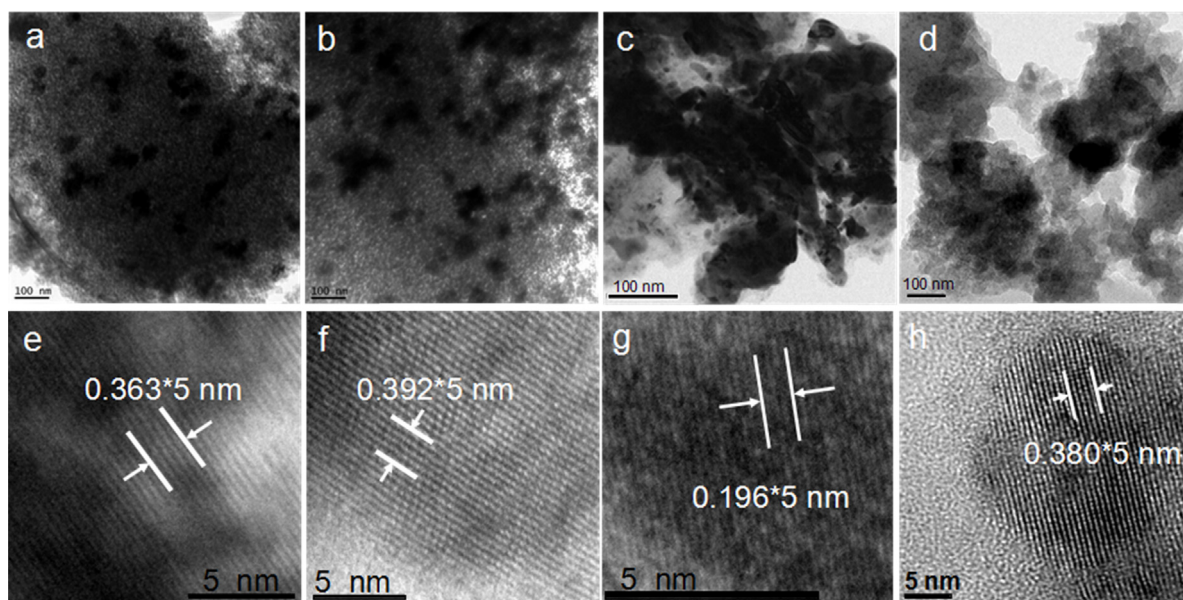Postmortem analysis of the used $WS–air$, $WS–N_2$, and $WS–1/1H_2/N_2$ was carried out to investigate the change in



**Fig. 6.** TEM (top) and HRTEM (bottom) images of $WS–N_2$ (a, e); $WS–1/1H_2/N_2$ (b, f); the used $WS–N_2$ (c, g); the used $WS–1/1H_2/N_2$ (d, h). Scale bars of (a), (b), (c), and (d) are 100 nm; scale bars of (e), (f), (g), and (h) are 5 nm.
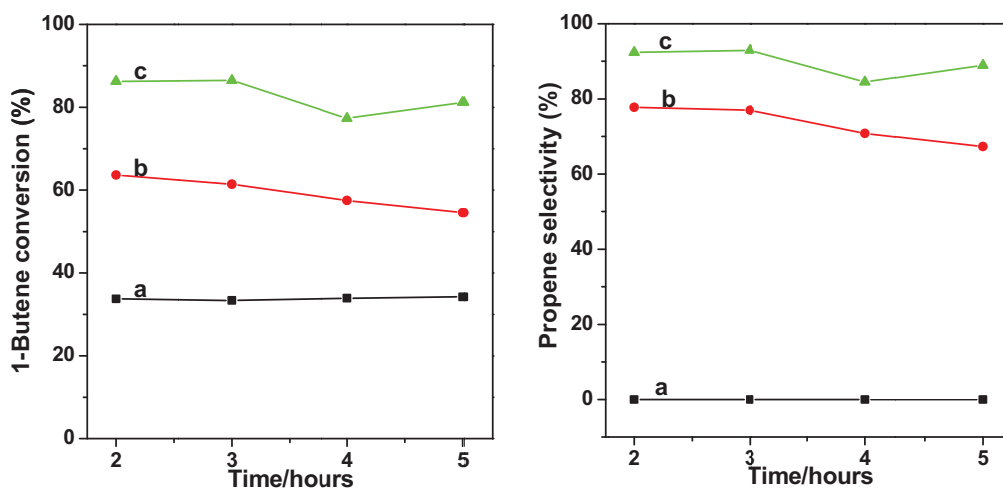
**Fig. 7.** (Color online.) 1-Butene conversion (left panel) and propene selectivity (right panel) over different catalysts: (a) MgO; (b) WS–1/1H$_2$/N$_2$; (c) WS–1/1H$_2$/N$_2$ + MgO. Reaction conditions: temperature: 280 °C; pressure: 3.0 MPa; C$_2$H$_4$ = 0.83 L/min and 1-C$_4$H$_8$ = 0.52 L/min; WO$_3$/SiO$_2$: 19.0 g; MgO: 76.0 g.

the physicochemical properties of the catalysts during the reaction. XRD patterns of the used catalysts are shown in Fig. 8. As shown in Fig. 8a, the used WS–air exhibited the same monoclinic WO$_3$ phase as WS–air before the reaction. In contrast, the WO$_3$ phase of WS–N$_2$ was gradually transformed from the monoclinic phase before the reaction (Fig. 1c) to the tetragonal phase after the reaction (Fig. 8b, 8c and 8d), suggesting the phase change during the reaction. Moreover, the WO$_3$ phase of WS–1/1H$_2$/N$_2$ transformed from the tetragonal phase before the reaction (Fig. 1e) to the WO$_{2.92}$ phase after the reaction (Fig. 8e), suggesting that the reactants or products could reduce the WO$_3$ phase under certain conditions. From the XRD data, it is inferred that the tetragonal WO$_3$ or partially reduced WO$_{3-x}$ phase were active phases. Furthermore, air-pretreated monoclinic WO$_3$ phase was stable and inactive, whereas the N$_2$-pretreated monoclinic WO$_3$ phase could be transformed into an active tetragonal WO$_3$ phase during the reaction.

The phase change of WS–N$_2$ and WS–1/1H$_2$/N$_2$ after the reaction was further confirmed by TEM studies. TEM images of the used WS–N$_2$ and WS–1/1H$_2$/N$_2$ are shown in Fig. 6c and 6d, respectively, and HRTEM images of the used WS–N$_2$ and WS–1/1H$_2$/N$_2$ are shown in Fig. 6 g and 6 h,

respectively. The lattice spacing with 0.196 nm in Fig. 6 g was consistent with that of (002) planes of the tetragonal WO$_3$, confirming the phase change from monoclinic WO$_3$ before the reaction to tetragonal WO$_3$ phase after the reaction for WS–N$_2$. Moreover, for the used WS–1/1H$_2$/N$_2$, the lattice spacing of 0.380 nm in Fig. 6 h was ascribed to that of (011) planes of WO$_{2.92}$, which is consistent with the phase change evidenced by the XRD pattern in Fig. 8e.

To investigate the oxidation state change of W species after the reaction, XPS studies of the used WS–air, WS–N$_2$, and WS–1/1 H$_2$/N$_2$ were conducted. As shown in Fig. 9a and Table 4, the used WS–air exhibited similar XPS data with WS–air before the reaction, showing the absence of reduced W$^{5+}$. However, XPS data of the used WS–N$_2$ collected at 20 min (Fig. 9b), 6 h (Fig. 9c), and 10 h (Fig. 9d) on stream illustrated the presence of a small portion of
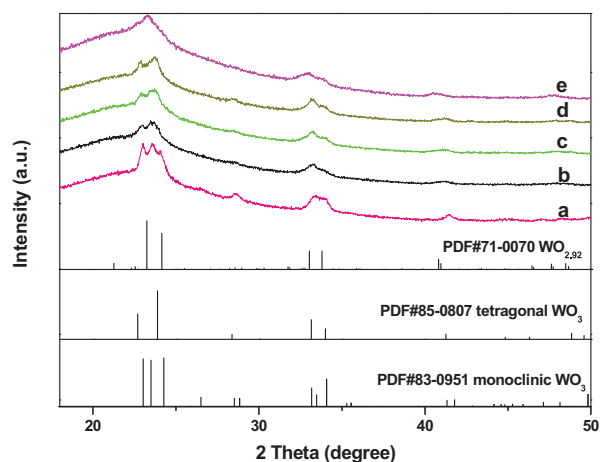
**Table 3**

Catalytic performances of MgO and WO$_3$/SiO$_2$ catalysts with different gas pretreatments for metathesis of 1-butene and ethene to propene.

| Catalysts[a] | 1-Butene conversion (%) | Selectivity (%) | |
|---|---|---|---|
| | | Propene | 2-Butene |
| MgO | 34.2 | 0.0 | 100.0 |
| WS–air + MgO | 33.5 | 0.0 | 100.0 |
| WS–N$_2$ + MgO | 75.0 | 84.1 | 15.9 |
| WS–1/9H$_2$/N$_2$ + MgO | 77.8 | 85.8 | 14.2 |
| WS–1/1H$_2$/N$_2$ + MgO | 86.3 | 92.3 | 7.7 |
| WS–H$_2$ + MgO | 83.4 | 90.5 | 9.5 |

[a] Reaction conditions: temperature: 280 °C; WHSV (1-butene + ethene) of 1.49 h$^{-1}$; pressure: 3.0 MPa; C$_2$H$_4$ = 0.83 L/min and 1-C$_4$H$_8$ = 0.52 L/min; WO$_3$/SiO$_2$: 19.0 g and MgO: 76.0 g; reaction time: 2 h.



**Fig. 8.** (Color online.) XRD patterns of 6.0 wt% WO$_3$/SiO$_2$ catalysts pretreated with different gases and collected after reaction testing: (a) the used WS–air, 10 h (after a 10-h reaction); (b) the used WS–N$_2$, 20 min; (c) the used WS–N$_2$, 6 h; (d) the used WS–N$_2$, 10 h; (e) the used WS–1/1H$_2$/N$_2$, 10 h.

**Table 4**
Binding energies and molar percentages of $W^{5+}$ and $W^{6+}$ species in the used $WO_3/SiO_2$ catalysts pretreated by different gases.

| Catalysts | Binding energies for $W_{4f}$ (eV) | | | | $W^{5+}$ (%) | $W^{6+}$ (%) |
|---|---|---|---|---|---|---|
| | $W^{6+}$ $4f_{5/2}$ | $W^{6+}$ $4f_{7/2}$ | $W^{5+}$ $4f_{5/2}$ | $W^{5+}$ $4f_{7/2}$ | | |
| WS–Air–10 h | 37.9 | 35.8 | N/A | N/A | 0.0 | 100.0 |
| WS–$N_2$–20 min | 38.0 | 35.9 | 36.7 | 34.6 | 5.0 | 95.0 |
| WS–$N_2$–6 h | 37.8 | 35.7 | 37.1 | 35.0 | 7.9 | 92.1 |
| WS–$N_2$–10 h | 37.9 | 35.8 | 36.8 | 34.7 | 14.3 | 85.7 |
| WS–$1/1H_2/N_2$–10 h | 38.2 | 36.1 | 37.1 | 35.0 | 17.8 | 82.2 |

$W^{5+}$, and the molar percentage of $W^{5+}$ increased from 5.0% at 20 min to 14.3% at 10 h, indicating the formation of some $W^{5+}$ during the reaction. The appearance of $W^{5+}$ for WS–$N_2$ during the reaction is consistent with the $H_2$-TPR data in Fig. 5, where WS–$N_2$ was easier to be reduced than WS–air. Moreover, the molar percentage of $W^{5+}$ of the used WS–$1/1H_2/N_2$ increased from 11.3% before the reaction in Table 2 to 17.8% after the reaction, as can be seen in Table 4, further confirming that the reactants or products in the metathesis of 1-butene and ethene can partially reduce $WO_3$.

The $W^{5+}$ content of WS–$N_2$ was significantly increased from 0.0% to 14.3% during the 10-h reaction, while the $W^{5+}$ content of WS–$1/1H_2/N_2$ was slowly increased from 11.3% to 17.8% during 10 h on stream. The significant increase in $W^{5+}$ for WS–$N_2$ may significantly influence the catalytic performance of WS–$N_2$ during the first several hours on stream if the $W^{5+}$ species were catalytically active. The catalytic studies mentioned above were carried out at 3.0 MPa and 280 °C in a 200-mL fixed-bed reactor with the 3–5-mm catalysts lumps. Under the above reaction conditions, 1-butene liquid at 3.0 MPa had to be pumped
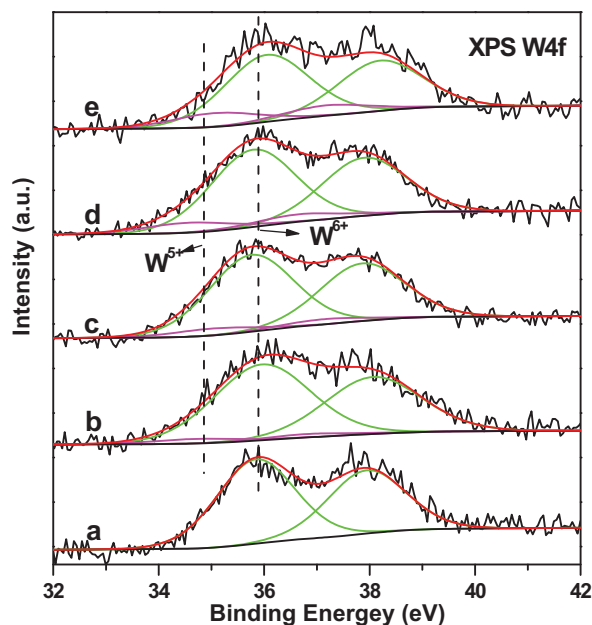


**Fig. 9.** (Color online.) XPS spectra of 6.0 wt% the used $WO_3/SiO_2$ catalysts pretreated with different gases and collected after reaction testing. (a) WS–air, 10 h (after a 10-h reaction); (b) WS–$N_2$, 20 min; (c) WS–$N_2$, 6 h; (d) WS–$N_2$, 10 h; (e) WS–$1/1H_2/N_2$, 10 h.

into a preheater to gasify. Because 1-butene contacted the catalyst layer later than ethene, the early stage of reaction cannot be correctly sampled and analyzed. To correctly investigate the initial stage of reaction, the reaction was carried out at 0.1 MPa and 430 °C in a 5-mL fixed-bed reactor with the 20–40 mesh catalysts. The 1-butene and
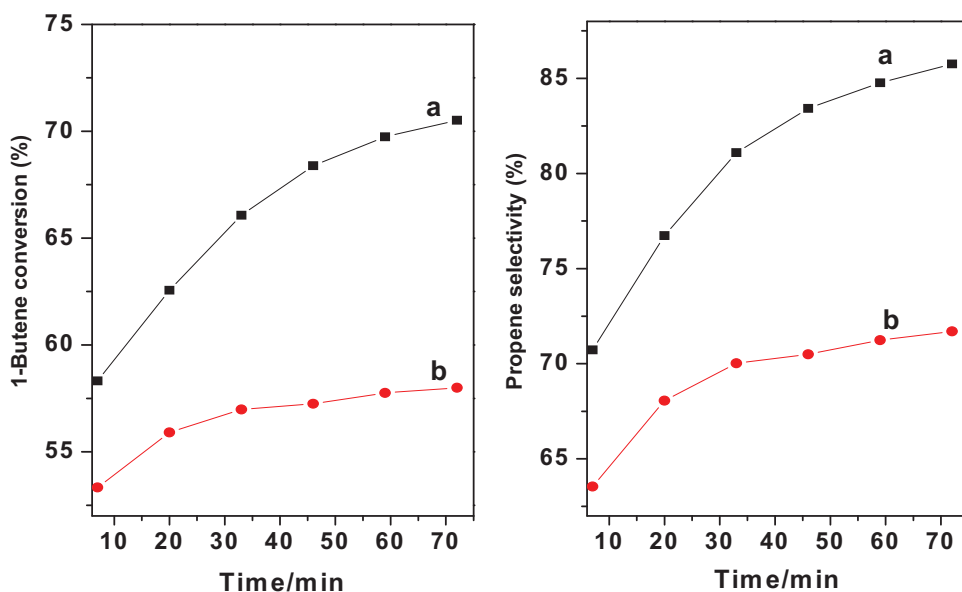


**Fig. 10.** (Color online.) 1-butene conversion (left panel) and propene selectivity (right panel) over different catalysts: (a) 1 g WS–$N_2$ + 1.5 g MgO; (b) 1 g WS–$1/1H_2/N_2$ + 1.5 g MgO. $T$ = 430 °C; P = 0.1 MPa; ethene, 10 mL/min; 1-butene, 5 mL/min.
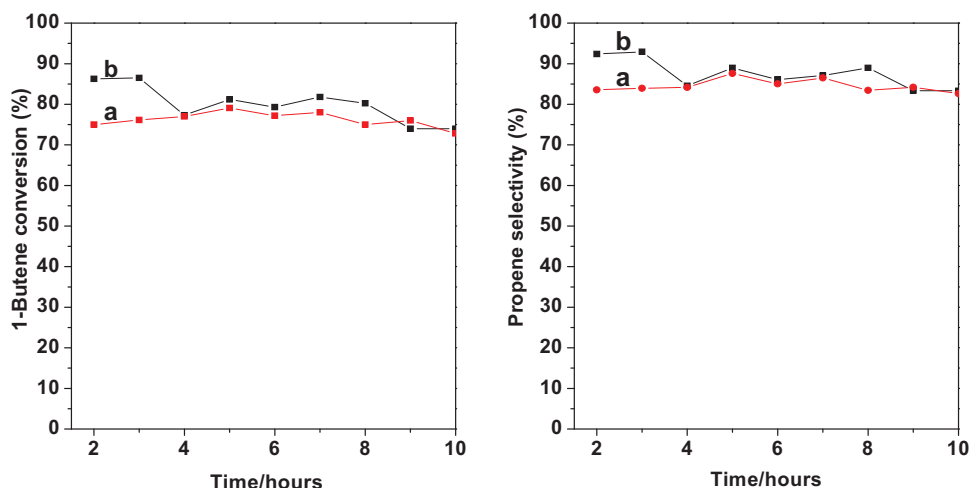
**Fig. 11.** (Color online.) The reaction profiles of 1-butene conversion (left panel) and propene selectivity (right panel) of gas-pretreated catalysts: (a) WS–$N_2$ + MgO; (b) WS–1/1$H_2$/$N_2$ + MgO. Reaction conditions: temperature, 280 °C; WHSV-(1-butene + ethene), 1.49 $h^{-1}$; $C_2H_4$ = 0.83 L/min and 1-$C_4H_8$ = 0.52 L/min; pressure, 3.0 MPa; $WO_3$/$SiO_2$, 19.0 g, and MgO, 76.0 g.

ethene at 0.1 MPa were fed into the reactor in a gas state so that the early stage of the reaction can be studied.

The initial catalytic performances at 0.1 MPa of WS–$N_2$ and WS–1/1$H_2$/$N_2$ in a microreactor are shown in Fig. 10. The reaction was carried out at 430 °C to clearly observe the catalytic performance change with the reaction time. As shown in Fig. 10b, 1-butene conversion and propene selectivity over WS–1/1$H_2$/$N_2$ increased slowly during the first 80 min. However, WS–$N_2$ exhibited a significant growth of catalytic activity and selectivity (Fig. 10a). The phase change from monoclinic to tetragonal by postmortem XRD study and the appearance of $W^{5+}$ during the reaction by postmortem XPS study can explain the significant activity growth during the early stage of

reaction for WS–$N_2$, and the tetragonal $WO_3$ phase and $W^{5+}$ were ascribed to the active phase and species. The appearance of $W^{5+}$ was necessary for the formation of sufficiently active and stable W carbene species responsible for metathesis [53,54]. Under these reaction conditions, WS–$N_2$ illustrated a better catalytic performance than WS–1/1$H_2$/$N_2$, suggesting that WS–$N_2$ was more suitable for high-temperature metathesis at 0.1 MPa.

The reaction profiles of 1-butene conversion and propene selectivity over WS–$N_2$ and WS–1/1$H_2$/$N_2$ are shown in Fig. 11. The reaction was again carried out at 3.0 MPa and 280 °C in a 200-mL fixed-bed reactor with the 3–5-mm catalysts lumps. The 1-butene conversion/propene selectivity of WS–1/1$H_2$/$N_2$ decreased from 86.3%/92.3%
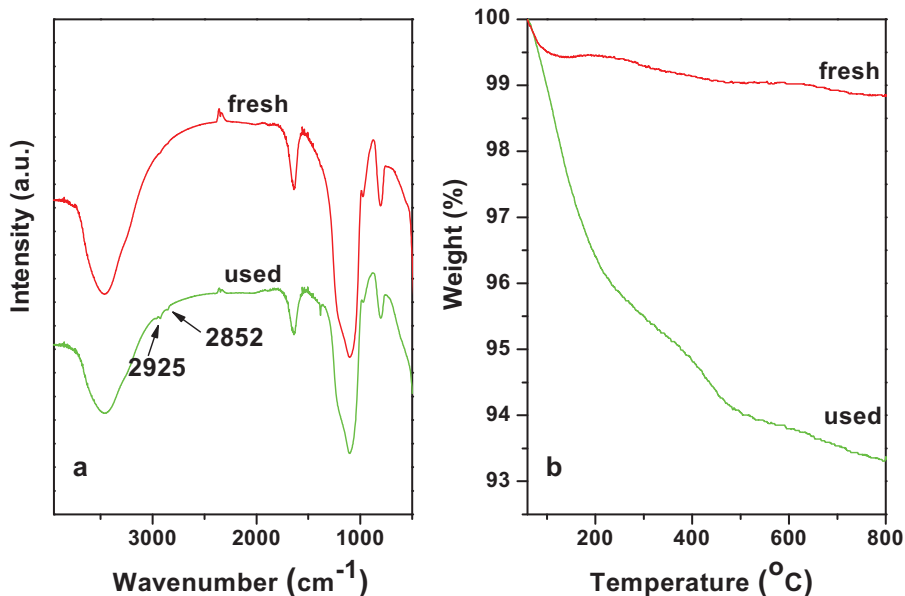


**Fig. 12.** (Color online.) (a) FT-IR spectra of the fresh and used WS–1/1$H_2$/$N_2$; (b) TGA profiles of the fresh and used WS–1/1$H_2$/$N_2$.

to 74.0%/83.3% after 10 h on stream. For comparison, the 1-butene conversion/propene selectivity of WS–$N_2$ decreased from 75%/83.5% to 72.8%/82.7% after 10 h on stream.

It should be emphasized here that the reaction conditions in this study were more critical than those in industrial processes. Pure 1-butene was used in this work, while industrial processes used mixtures of 1-butene and 2-butene, and 2-butene was more favorable to the metathesis of butene and ethene to propene [55–58].

In the literature, the deep reduction of $WO_x$ was found to be unfavorable to metathesis [28,51]. In this study, the XRD patterns of the used WS–1/1$H_2$/$N_2$ revealed the formation of a $WO_{2.92}$ phase after the reaction. Therefore, no deep reduction occurred.

FT-IR spectra and TGA profiles of the fresh and used WS–1/1$H_2$/$N_2$ are illustrated in Fig. 12. Some organic residues on the catalyst were indicated by the appearance of the antisymmetric stretching vibration of the methyl group at 2925 cm$^{-1}$ in FT-IR spectra of the used catalyst in Fig. 12a [59]. Moreover, TGA analysis in Fig. 12b provides another evidence of organic residues on the used catalyst. Compared with the fresh catalyst, an additional 5.5 wt% of weight loss of the used catalyst was observed. The catalyst's deactivation is possibly due to the deposition of heavy organic compounds onto catalysts during the reaction.

## 4. Conclusions

$WO_3$/$SiO_2$ catalysts pretreated by air, $N_2$, 1/9$H_2$/$N_2$, 1/1$H_2$/$N_2$ and pure $H_2$ were characterized by XRD, $N_2$ adsorption–desorption, Raman, UV–vis, TGA, FT-IR, TEM, XPS and $H_2$-TPR, and tested in the metathesis of 1-butene and ethene to propene. WS–air with monoclinic $WO_3$ phase was inactive, and the monoclinic $WO_3$ phase cannot be transformed into an active phase during the reaction. WS–$N_2$, WS–$H_2$/$N_2$, and WS–$H_2$ showed enhanced catalytic performance. The tetragonal $WO_3$ and partially reduced $WO_{2.92}$ were active phases for the reaction. The tetragonal $WO_3$ phase can be formed by pretreatment in $H_2$/$N_2$ mixtures or from the transformation of monoclinic $WO_3$ of WS–$N_2$ during the reaction. All active $WO_3$/$SiO_2$ catalysts after the reaction contained $W^{5+}$ species, which are assigned to active W species.

It should be cautioned that the conclusion about the active W species and crystallographic phases may be dependent on the $SiO_2$ nature of the support, which may not be the case with other supported catalysts. In addition, the characterization in our study was conducted ex situ, but not in situ. The interaction between the reactants/intermediates and the active sites may be dynamic during the reaction. Additional work is still needed to better understand the reaction mechanism.

As for the implication of the current work to industrial catalysis, we would like to propose that perhaps the pretreatment conditions (i.e., pretreatment gas, temperature, duration of pretreatment) should be strictly controlled to get the best performance in olefin metathesis. In addition, the option of using in situ activation of catalysts (i.e., for WS–$N_2$ during the reaction) should be avoided, just in order to get stable activity and selectivity in industrial reactors.

## References

[1] R.L. Banks, G.C. Bailey, Ind. Eng. Chem. Prod. Res. Dev. 3 (1964) 170–173.
[2] R.R. Schrock, Angew. Chem. Int. Ed. 45 (2006) 3748–3759.
[3] R.H. Grubbs, Angew. Chem. Int. Ed. 45 (2006) 3760–3765.
[4] Y. Chauvin, Angew. Chem. Int. Ed. 45 (2006) 3740–3747.
[5] K.J. Ivin, J.C. Mol, Olefin metathesis and metathesis polymerization, 2nd ed., Academic Press, London, 1997.
[6] J.C. Mol, J. Mol. Catal. A: Chem. 213 (2004) 39–45.
[7] R.H. Grubbs, T.K. Brunck, J. Am. Chem. Soc. 94 (1972) 2538–2540.
[8] V.M. Benitez, C.A. Querini, N.S. Figoli, Appl. Catal. A 252 (2003) 427–436.
[9] D. Lokhat, M. Starzak, M. Stelmachowski, Appl. Catal. A 351 (2008) 137–147.
[10] D.P. Debecker, B. Schimmoeller, M. Stoyanova, C. Poleunis, P. Bertrand, U. Rodemerck, E.M. Gaigneaux, J. Catal. 277 (2011) 154–163.
[11] X.J. Li, W.P. Zhang, S.L. Liu, L.Y. Xu, X.W. Han, X.H. Bao, J. Phys. Chem. C 112 (2008) 5955–5960.
[12] X. Teng, D.R. Cefalo, R.R. Schrock, A.H. Hoveyda, J. Am. Chem. Soc. 124 (2002) 10779–10784.
[13] L.G. Duquette, R.C. Cieslinsky, C.W. Jung, P.E. Garrou, J. Catal. 90 (1984) 362–365.
[14] B. Mitra, X. Gao, I.E. Wachs, A.M. Hirt, G. Deo, Phys. Chem. Chem. Phys. 3 (2001) 1144–1152.
[15] J.C. Mol, Catal. Today 51 (1999) 288–289.
[16] R. Spronk, J.A.R. Vanveen, J.C. Mol, J. Catal. 144 (1993) 472–483.
[17] R.L. Banks, Appl. Ind. Catal. 4 (1984) 215.
[18] A. Rodriguez-Ramos, Guerrero-Ruiz, N. Horns, P.P. Ramirezdela, J.L.G. Fierro, J. Mol. Catal. A: Chem. 95 (1995) 147–154.
[19] W. Michael McCaulley, US 5300718 1994.
[20] R.C. Luckner, G.B. Wills, J. Catal. 28 (1973) 83–91.
[21] S.K. Gangwal, J. Fathi-kalajahi, G.B. Wills, Ind. Eng. Chem. Prod. Res. Dev. 16 (1977) 193–268.
[22] F. Pennella, R.L. Banks, J. Catal. 31 (1973) 304–308.
[23] A. Andreini, J.C. Mol, J. Colloid Interface Sci. 84 (1985) 57–65.
[24] R. Thomas, J.A. Moulijn, J. Mol. Catal. 8 (1980) 161–174.
[25] S.J. Choung, S.W. Weller, Ind. Eng. Chem. Prod. Res. Dev. 22 (1983) 662–665.
[26] R. Westhoff, J.A. Moulijn, J. Catal. 46 (1977) 414–416.
[27] A.G. Basrur, S.R. Patwardhan, S.N. Was, J. Catal. 127 (1991) 86–95.
[28] S.J. Huang, S.L. Liu, W.J. Xin, J. Bai, S.J. Xie, Q.X. Wang, L.Y. Xu, J. Mol. Catal. 226 (2005) 61–68.
[29] M.I. Zaki, N.E. Fouad, S.A.A. Mansour, A.I. Muftah, Thermochim. Acta 523 (2011) 90–96.
[30] E. Lassner, W.-D. Schubert, Tungsten: properties, chemistry, technology of the element, alloys, and chemical compounds, Kluwer Academic/Plenum Publishers, New York, 1999.
[31] Q.F. Zhao, S.L. Chen, J.S. Gao, C.M. Xu, Transit. Metal Chem. 34 (2009) 621–627.
[32] S. Doniach, M. Sunjic, J. Phys. C: Solid State Phys. 3 (1970) 285–291.
[33] P. Biloen, G.T. Pott, J. Catal. 30 (1973) 169–174.
[34] X.L. Yang, W.L. Dai, R.H. Gao, K.N. Fan, J. Catal. 249 (2007) 278–288.
[35] M. Valigi, D. Gazzoli, I. Pettiti, G. Mattei, S. Colonna, S.D. Rossi, G. Ferraris, Appl. Catal. A 231 (2002) 159–172.
[36] P. Charton, L. Gengembre, P. Armand, J. Solid State Chem. 168 (2002) 175–183.
[37] A.P. Shpak, A.M. Korduban, M.M. Medvedskij, V.O. Kandyba, J. Electron. Spectrosc. Relat. Phenom. 156 (2007) 172–175.
[38] M.S. Bazarjani, M. Hojamberdiev, K. Morita, G.Q. Zhu, G. Cherkashinin, C. Fasel, T. Herrmann, H. Bretzke, A. Gurlo, R. Riede, J. Am. Chem. Soc. 135 (2013) 4467–4475.
[39] R.J. Colton, A.M. Guzman, J.W. Rabalais, Acc. Chem. Res. 11 (1978) 170–176.
[40] E.L. Lee, I.E. Wachs, J. Phys. Chem. C 112 (2008) 6487–6489.
[41] F. Figueras, J. Palomeque, S. Loridant, C. Fèche, N. Essayem, G. Gelbard, J. Catal. 226 (2004) 25–31.

[42] L. Salavati Jr., L.E. Makovsky, J.M. Stencel, F.R. Brown, D.M. Hercules, J. Phys. Chem. 85 (1981) 3700–3707.

[43] E.I. Ross-Medgaarden, W.V. Knowles, T. Kim, M.S. Wong, W. Zhou, C.J. Kiely, I.E. Wachs, J. Catal. 256 (2008) 108–125.

[44] J.A. Horsely, I.E. Wachs, J.M. Brown, G.H. Via, F.D. Hardcastle, J. Phys. Chem. 91 (1987) 4014–4020.

[45] G.M. Wang, Y.C. Ling, H.Y. Wang, X.Y. Yang, C.C. Wang, J.Z. Zhang, Y. Li, Energy Environ. Sci. 5 (2012) 6180–6187.

[46] J.G. Liu, Y. Zhao, Z.J. Zhang, J. Phys.: Condens. Matter 15 (2003) L453.

[47] A. Ramanathan, B. Subramaniam, D. Badloe, U. Hanefeld, R.M. Maheswari, J. Porous Mater. 19 (2012) 961–968.

[48] X.L. Yang, R.H. Gao, W.L. Dai, K.N. Fan, J. Phys. Chem. C 112 (2008) 3819–3826.

[49] J. Ramirez, A.G. Alejandre, J. Catal. 170 (1997) 108–122.

[50] H.L. Wang, T. Lindgren, J.J. He, A. Hagfeldt, S.E. Lindquist, J. Phys. Chem. B 104 (2000) 5686–5696.

[51] A. Spamer, T.I. Dube, D.J. Moodley, C.V. Van, J.M. Botha, Appl. Catal. A 255 (2003) 133–142.

[52] B. Hu, H. Liu, K. Tao, C.R. Xiong, S.H. Zhou, J. Phys. Chem. 117 (2013) 26385–26395.

[53] B. Zhang, N. Liu, Q.S. Lin, D. Jin, J. Mol. Catal. 65 (1991) 15–28.

[54] B.N. Shelimov, L.V. Elev, V.B. Kazansky, J. Catal. 98 (1986) 70–81.

[55] D.R. Hua, S.L. Chen, G.M. Yuan, Y.L. Wang, L. Zhang, Transit. Metal Chem. 36 (2011) 245–248.

[56] K. Weiss, G. Lössel, Angew. Chem. Int. Ed. 28 (1989) 62–64.

[57] M. Taoufik, E.L. Roux, J. Thivolle-Cazat, J.M. Basset, Angew. Chem. Int. Ed. 46 (2007) 7202–7205.

[58] E. Mazoyer, K.C. Szeto, S. Norsic, A. Garron, J.M. Basset, C.P. Nicholas, M. Taoufik, ACS Catal. 1 (2011) 1643–1646.

[59] T. Noguchi, M. Sugiura, Biochem. 42 (2003) 6035–6042.